FORCE MODELING UNDER DEAD METAL ZONE EFFECT IN ORTHOGONAL CUTTING WITH CHAMFERED TOOLS

Yu Long, Yong Huang
Department of Mechanical Engineering
Clemson University
Clemson, South Carolina

KEYWORDS

Force Modeling, Chamfered Tool, Dead Metal Zone, Orthogonal Cutting

ABSTRACT

Chamfered tools are finding broad applications in interrupted cutting as well as cutting hard materials since they offer good cutting toughness, edge chipping/breakage resistance, and energy efficiency. A better understanding of the cutting process using chamfered tools will help select proper cutting conditions and tool geometry. Since the dead metal zone is frequently reported in cutting with chamfered tools, its effect on the cutting process needs to be understood. This study proposes a new force modeling approach to include the dead metal zone effect based on a three-zone model. Satisfactory match between the predictions and the measurements has been achieved. An improved modeling accuracy is also observed when compared with a previous modeling effort. The proposed method will help better design chamfered tools as well as optimize their usage.

NOMENCLATURE

A, B, C, D, E, m, n	Constants of the Johnson-Cook equation
C_{MN}	Shear strain rate constant of the primary shear zone
F_1, F_2	Shear forces on the effective rake face and on the bottom edge of DMZ
F_{c1}, F_{c2}	Cutting forces of the primary shear zone and on the bottom edge of DMZ
F_{t1}, F_{t2}	Thrust forces of the primary shear zone and on the bottom edge of DMZ
$h, w,$ $\lambda_{chamfer}$	Contact length along the tool-chip interface, width of cut, and chamfer length
k, k_{chip}, k_{MN}, k_{p3}	Shear flow stresses (along the tool-chip interface, of the primary shear zone, and along the DMZ-extruded workpiece interface)
K, S, ρ	Thermal conductivity, specific heat, and density of workpiece
N_1, N_2	Normal forces on the rake face and on the DMZ bottom edge
R	Resultant force on the rake face
s_2	Primary shear zone thickness
$t_0, t_{chip},$ t_{e1}, t_{e2}	Undeformed chip thickness, chip thickness, and effective up/down flowing undeformed chip thicknesses
T_m	Workpiece melting temperature
$u_{p1,2,3}$	Specific energies of extrusion, excess, friction deformation
$V, V_{chip} V_s$	Cutting speed, chip velocity, and

	shear velocity
V_{under}	Material velocity under the DMZ
$\alpha, \beta, \phi, \theta$	Rake angle, chamfer angle, shear angle, and inclination angle of R to the primary shear zone
γ	Angle between the bottom of DMZ and the cutting direction
γ_{MN}, $\dot{\gamma}_{MN}$	Shear strain and shear strain rate along the primary shear plane
δ_1, δ_2	Thickness ratio of thin layer along the tool-chip interface to the chip thickness and that along the DMZ-workpiece interface to the deformed zone thickness
$\Delta time$	Time taken for the workpiece to pass under the DMZ
$\Delta T_{chip}, \Delta T_{MN}$, ΔT_{work}	Average temperature rises in the chip, of the primary shear zone, and of the zone under the DMZ
$\dot{\varepsilon}_{\text{int}}$	tool-chip interface strain rate
ε, $\varepsilon_{MN}, \dot{\varepsilon}_{MN}$	Strain, strain and strain rate along the primary shear zone
$\varepsilon_{p1}, \dot{\varepsilon}_{p1}$, $\varepsilon_{p2}, \dot{\varepsilon}_{p2}$	Strains and strain rates of the extrusion/excess deformations
$\dot{\varepsilon}_{p3}$	Strain rate of friction deformation
η, λ	Friction angles on the DMZ bottom edge and of rake face
σ, σ_{N1}, $\sigma'_{N1}, \sigma_{N2}$, σ'_{N2}	Normal stresses (on the effective rake face and the bottom of DMZ)
τ_{int}	Tool-chip interface shear stress

INTRODUCTION

Machining is a common material removal process, and the United States alone spends some $300 billion per year in machining (Komanduri, et al., 2001). To improve the cutting process efficiency and effectiveness, the tool geometry should be carefully designed in addition to the optimization of cutting conditions. As a result of such efforts, chamfered tools were first introduced in Japan (Hitomi, 1961). Such chamfered tools can offer good cutting toughness and edge chipping/breakage resistance, and they also decrease the energy consumption and prolong the tool life (Shaw, 1984). Due to their attractive properties, recently chamfered tools are finding broad applications in interrupted cutting (Hirao, et al., 1982) as well as cutting hard materials (Huang, 2002).

Typical chamfered tools have a negative chamfer angle from -10 to -25 degrees. Since the chamfer edge (land) is mainly responsible for material removal, the dead metal zone (DMZ) has been frequently reported in cutting (Hirao, et al., 1982; Jacobson, et al., 1988; and Zhang, et al., 1991) as in cutting with large negative rake angle tools (Lortz, 1979; Abebe, et al., 1981; and Kita, et al., 1982). The DMZ is a zone filled with a trapped volume of stagnant dead metal before the chamfered edge. It differs from the built-up edge (BUE) formed before the tool tip since BUE is an unstable structure and breaks up eventually.

Although Hitomi (1961) and Chang et al. (1998) reported that the workpiece materials formed under such a chamfer edge are removed as the secondary chip, it was more frequently observed that they form a stagnant dead metal zone and this zone acts as an additional cutting edge (Jacobson, et al., 1988; Hirao, et al., 1982; and Zhang, et al., 1991). Besides the experimental efforts for better design of chamfered tools, some notable analytical work has been made to provide a better understanding on their cutting mechanism. Zhang et al. (1991) proposed a three-zone (primary, tool-chip interface/secondary, and dead metal deformation zones) cutting model and solved the shear angle based on the minimum energy principle. Ren et al. (2000) further developed this three-zone model (Zhang, et al., 1991) by using Oxley's predictive machining theory (Oxley, 1989) to model the primary and secondary deformation zones. A power-law material model was used to predict the material behavior in the modeling approach (Ren, et al., 2000). Recently, Movahhedy et al. (2002) proposed a finite element based numerical analysis to model the continuous chip formation process in cutting with chamfered tools. They found that a stagnant material zone under the chamfer edge is evident in simulation results and chamfer angle does not affect the chip removal process significantly.

For better application of chamfered tools in interrupted cutting and cutting advanced materials, there is an increasing need to further the understanding of the chamfered tool cutting mechanism. The objective of this study is to continue such a need in modeling the chamfer tool cutting process. Since theoretical modeling provides more physical insights on process fundamentals and is much less time consuming

than numerical approaches, it is favored in this study. This study continues the previous theoretical efforts (Zhang, et al., 1991; and Ren, et al., 2000) in modeling chamfered tool cutting forces by 1) determining the angle between the DMZ bottom edge and the cutting direction (γ) by minimizing the total energy in cutting instead of assuming a simple relationship between γ and the shear angle as in (Zhang, et al., 1991; and Ren, et al., 2000); 2) using the extension of the tool main rake face to define the DMZ cutting edge as observed in (Hirao, et al., 1982; and Jacobson, et al., 1988), which was taken as vertical in (Zhang, et al., 1991; and Ren, et al., 2000); 3) finding the size of the deformation zone under the DMZ bottom edge by using an effective friction angle; and 4) formulating a modeling approach based on the Johnson-Cook constitutive equation, which is more general than other flow stress models. The following sections discuss the detailed modeling approach and the model validation in cutting P20 mold steel, and the paper ends with conclusions.

FORCE MODELING IN ORTHOGONAL CUTTING USING CHAMFERED TOOLS

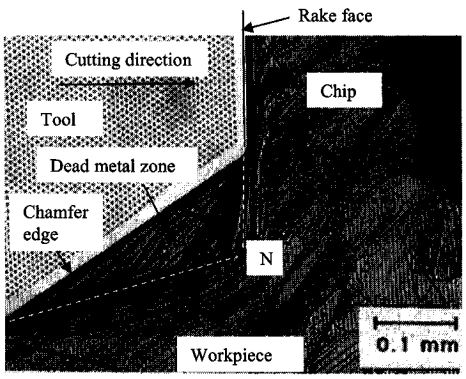

FIGURE 1. A SCHEMATIC OF THE DMZ BASED ON AN EXPERIMENTAL OBSERVATION (JACOBSON, ET AL., 1988).

A typical DMZ shown in Fig. 1 is drawn based on an experimental observation in (Jacobson, et al., 1988). The stagnant dead metal under the chamfer edge forms a cutting edge with a stagnation point N at the tip of the DMZ. The cross sectional area of the DMZ is normally taken as triangular in theoretical analysis for simplicity (Zhang, et al., 1991). The workpiece material flows upward above point N, and it flows downward underneath the DMZ if below point N. For typical chamfered tools with a rake angle between 0—±5°, the DMZ cutting edge can be approximated as the extension from the tool rake face based on the observations in (Hirao, et al., 1982; and Jacobson, et al., 1988), and this is taken as an assumption in this study for simplification. This cutting geometry simplification was also adopted in modeling the cutting mechanism of edge honed tools with a stable build-up material adhered to the edge (Waldorf, et al., 1998, 1999).

Based on the above simplifications, the plastic deformation in cutting is considered from three zones: the primary and the secondary zones due to the tool main rake face and the DMZ cutting edge, and the extrusion zone due to the DMZ boundary below the stagnation point. This proposed cutting geometric model in orthogonal cutting and its hodograph are shown in Figures 2 and 3 respectively. As pointed in (Ren, et al., 2000), an extrusion analogy for the plastic flow under the DMZ may not be the same as that observed in machining since indentation (Waldorf, et al., 1999) is not considered. However, this approach will give a first approximation to the ploughing process under the DMZ, so the extrusion analogy for the DMZ effect is used in this study as in (Zhang, et al., 1991; and Ren, et al., 2000).

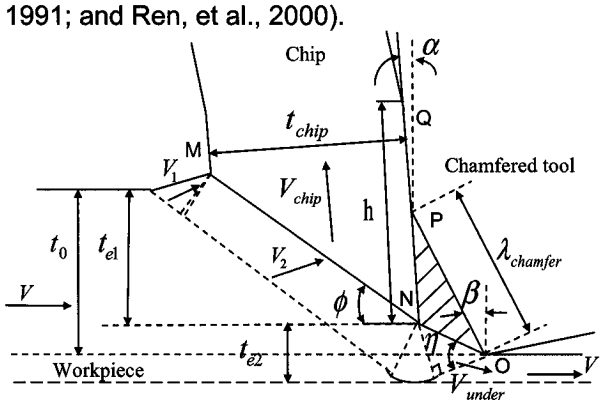

FIGURE 2. PROPOSED MODEL OF CUTTING GEOMETRY.

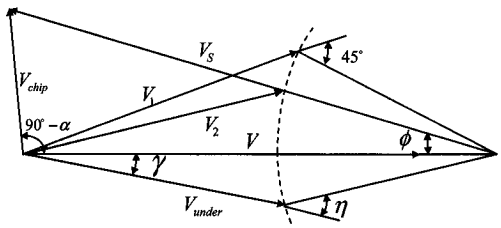

FIGURE 3. CUTTING MODEL HODOGRAPH.

Plastic Deformation in Primary Shear Zone

As in (Oxley, 1989; and Huang, et al., 2003),

the detailed velocities such as V_1 and V_2 are ignored, and the primary shear zone is considered as a plane which is defined by the line MN in Fig 2. Since the total undeformed chip thickness t_0 is divided into two parts: a part represented by a thickness t_{e1} flowing up forward and the other flowing below the DMZ. t_{e1} can be calculated as follows:

$$t_{e1} = t_0 - \frac{\lambda_{chamfer} \sin\gamma \sin(\alpha-\beta)}{\cos(\alpha-\gamma)} \quad (1)$$

Under this orthogonal cutting setup, the basic process relationships can be given as:

$$t_{chip} = t_{e1}\cos(\phi-\alpha)/\sin\phi \quad (2)$$

$$\varepsilon_{MN} = \frac{\gamma_{MN}}{\sqrt{3}} = \frac{\cos\alpha}{2\sqrt{3}\sin\phi\cos(\phi-\alpha)} \quad (3)$$

$$F_{c1} = R\cos(\lambda-\alpha), \quad F_{t1} = R\sin(\lambda-\alpha) \quad (4)$$

$$R = \frac{k_{MN} t_{e1} w}{\sin\phi\cos\theta} \quad (5)$$

$$\lambda = \alpha + \theta - \phi \quad (6)$$

$$\tan\theta = 1 + 2(\frac{\pi}{4} - \phi) - \left(\frac{dk}{ds_2}\right)_{MN} \frac{t_{e1}}{2k_{MN}\sin\phi} \quad (7)$$

where, $\left(\frac{dk}{ds_2}\right)_{MN}$ is the variation in the shear flow stress across the width of the parallel-sided shear zone, and it is calculated as (Oxley, 1989; and Huang, et al., 2003):

$$\left(\frac{dk}{ds_2}\right)_{MN} = \left(\frac{dk}{d\gamma}\right)_{MN}\left(\frac{d\gamma}{dt}\right)_{MN}\left(\frac{dt}{ds_2}\right)_{MN} \quad (8)$$

$$\left(\frac{d\gamma}{dt}\right)_{MN} = C_{MN}\frac{V_s\sin\phi}{t_{e1}} = C_{MN}\frac{V\cos\alpha\sin\phi}{\cos(\phi-\alpha)t_{e1}} \quad (9)$$

$$\left(\frac{dt}{ds_2}\right)_{MN} = \frac{1}{V\sin\phi} \quad (10)$$

As a more general constitutive law, the Johnson-Cook equation is used in modeling the workpiece constitutive relationship as:

$$\sigma = (A + B\varepsilon^n)\left(1 + C\log\frac{\dot{\varepsilon}}{\dot{\varepsilon}_0}\right)\left(D - E(T^*)^m\right) \quad (11)$$

where: $T^* = \frac{T - T_0}{T_m - T_0}$, T_0 is normally taken as 20°C and $\dot{\varepsilon}_0$ as 1.0, and T is any local temperature.

Based on the Johnson-Cook equation, $\left(\frac{d\sigma}{d\varepsilon}\right)_{MN}$ is computed as follows (Ramesh, 2002; and Huang, et al., 2003):

$$\left(\frac{dk}{d\gamma}\right)_{MN} = \frac{1}{3}\left(\frac{d\sigma}{d\varepsilon}\right)_{MN} = \frac{1}{3}\left(\frac{\partial\sigma}{\partial\varepsilon} + \frac{\partial\sigma}{\partial T}\frac{dT}{d\varepsilon}\right)_{MN} \quad (12)$$

Then $\tan\theta$ is further calculated as Equ. (7) based on known $\left(\frac{dk}{ds_2}\right)_{MN}$.

The temperature value inside this primary shear zone in this study is determined base on the empirical equations in (Oxley, 1989). The normal stress σ'_{N1} can be found from the boundary condition at point N for the normal stress distribution along MN (Oxley, 1989; and Huang, et al., 2003):

$$\sigma'_{N1} = k_{MN}\left(1 + \frac{\pi}{2} - 2\alpha - \left(\frac{dk}{ds_2}\right)_{MN}\frac{t_{e1}}{\sin\phi}\right) \quad (13)$$

Plastic Deformation in Tool-Chip Interface

For the assumed normal stress distribution, the contact length h along the tool-chip interface is estimated based on Oxley's approach (Oxley, 1989) as follows:

$$h = \frac{4t_{e1}\sin\theta}{\cos\lambda\sin\phi}\frac{p_M/3 + p_N/6}{p_M + p_N} \quad (14)$$

where, hydrostatic stresses $p_M = k_{MN}\left(1 + \frac{\pi}{2} - 2\phi\right)$ and $p_N = p_M - \left(\frac{dk}{ds_2}\right)_{MN}\frac{t_{e1}}{\sin\phi}$.

The strain-rate at the tool-chip interface can be represented as follows (Oxley, 1989):

$$\dot{\varepsilon}_{\text{int}} = \frac{V_{chip}}{\sqrt{3}\delta_1 t_{chip}} \quad (15)$$

By calculating the temperature information T_{int} in the tool-chip interface zone and ignore the negligible strain-hardening effect as in (Oxley, 1989), the shear flow stress in the chip adjacent to the interface can be calculated based on the modified Johnson-Cook equation as (Huang, et al., 2003):

$$k_{chip} = \frac{A}{\sqrt{3}}(1 + C\log\dot{\varepsilon}_{\text{int}})(D - E(T_{\text{int}}^*)^m) \quad (16)$$

The stress distribution is assumed uniform along the tool-chip interface. The average normal stress σ_{N1} and shear stress τ_{int} at the tool-chip interface are given by:

$$\sigma_{N1} = \frac{N_1}{hw}, \quad \tau_{\text{int}} = \frac{F_1}{hw} \quad (17)$$

Plastic Deformation under DMZ

The workpiece below the tip of the DMZ flows underneath the DMZ boundary NO, and this process is simplified here as an extrusion process (Zhang, et al., 1991). As shown in Figure 4, the total energy consumed in this extrusion process includes: extrusion deformation energy, excess deformation energy at both entrance and exit of the deformation zone, and friction energy consumed along the DMZ boundary NO. The deformation zone under the DMZ is determined based on an effective friction angle η, which is estimated from:

$$\tan \eta = \frac{F_2}{N_2} \tag{18}$$

where, $F_2 = \frac{k_{p3} w \lambda_{chamfer} \sin(\alpha - \beta)}{\cos(\alpha - \gamma)}$ (k_{p3} as in Equ. (32)), $N_2 = \frac{\sigma_{N2} \lambda_{chamfer} w \sin(\alpha - \beta)}{\cos(\alpha - \gamma)}$, and σ'_{N2} is found by turning the primary shear line through an angle $\pi/2 + \phi - \gamma$ as in (Waldorf, et al., 1998).

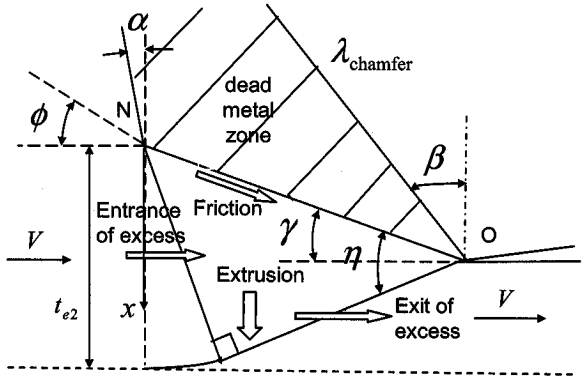

FIGURE 4. GEOMETRY ILLUSTRATION OF THE DEFORMATION ZONE UNDER THE DMZ.

The zone is approximately considered as a triangular zone based on η and the slip line model. The effective undeformed down flowing chip thickness can be computed as:

$$t_{e2} = \frac{\lambda_{chamfer} \sin(\alpha - \beta) \sin \eta}{\cos(\alpha - \gamma)} \tag{19}$$

The total volume passing below the DMZ is equal to $t_{e2} w V$, and the cutting forces coming from the bottom edge of the DMZ is as follows:

$$F_{c2} = F_2 \cos\gamma + N_2 \sin\gamma, \quad F_{t2} = N_2 \cos\gamma - F_2 \sin\gamma \tag{20}$$

Temperature rises of the material below the DMZ are required to estimate the flow stress information. By assuming no heat loss, the temperature rise of the bulk workpiece material flowing underneath the DMZ is considered uniformly distributed as:

$$\Delta T_{work} = \frac{\xi (u_{p1} + u_{p2} + u_{p3})}{\rho S} \tag{21}$$

where, ξ is the fraction of deformation energy converted into heat during this process, and is typically taken as 0.9. The total energy consumption under the DMZ zone is due to excess (u_{p1}), extrusion (u_{p2}), and friction (u_{p3}), and the specific energies per unit volume and unit time are discussed in the following sections, respectively.

The bulk temperature T_{bulk} is calculated as $T_r + \Delta T_{MN} + \Delta T_{work}$. The maximum temperature rise ΔT_{wMax} along the DMZ boundary is predicted based on the known ΔT_{work} as (Zhang, et al., 1991):

$$\log\left(\frac{\Delta T_{wMax}}{\Delta T_{work}}\right) = 0.06 - 0.195\delta_2 \left(\frac{R_{wT}}{\sin\eta}\right)^{0.5} + 0.5 \log\left(\frac{R_{wT}}{\sin\eta}\right) \tag{22}$$

where, $R_{wT} = V t_{e2} \rho S / K$. The temperature rise along the DMZ boundary T_b is known as $T_r + \Delta T_{MN} + 0.9 \Delta T_{wMax}$ (Zhang, et al., 1991).

Specific Energy in Extrusion Deformation.

The strain in the extrusion part is calculated as:

$$\varepsilon_{p1} = \frac{\sin\gamma}{\sin\eta} \tag{23}$$

In estimating the strain rate, it is proposed that the workpiece material deforms uniformly during the process (Zhang, et al., 1991), so the strain rate is estimated as:

$$\dot{\varepsilon}_{p1} = \frac{\varepsilon_{p1}}{\Delta time} \tag{24}$$

where; the time consumed in the change of strain is defined as:

$$\Delta time = \frac{\lambda_{chamfer} \sin(\alpha - \beta) \sin\eta}{V \cos(\alpha - \gamma) \sin(\gamma + \eta)} \tag{25}$$

By considering the constant strain rate and the uniform temperature distribution during deformation, the specific energy for the extrusion deformation is calculated as:

$$u_{p1} = \left(A\varepsilon_{p1} + \frac{B\varepsilon_{p1}^{(n+1)}}{n+1} \right) (1 + C \log\dot{\varepsilon}_{p1})(D - E(T_{bulk}^{*})^m) \tag{26}$$

Specific Energy in Excess Deformation.

Excess deformation in cutting is contributed by

the interior shear deformation (Zhang, et al., 1991), and consumes energy in overcoming this interior shear. The strain of excess part can be estimated as (Zhang, et al., 1991):

$$\varepsilon_{p2} = \frac{\tan\gamma}{\sqrt{3}} \tag{27}$$

Similar as in computing the extrusion strain rate, the excess strain rate is approximated as:

$$\dot{\varepsilon}_{p2} = \frac{\varepsilon_{p2}}{\Delta time} \tag{28}$$

Also by considering the constant strain rate and the uniform temperature distribution during deformation, the specific energy of the entrance $u_{p2entrance}$ is given as follows:

$$u_{p2entrance} = \frac{1}{t_{e2}} \int_0^{t_{e2}} \int_0^{\varepsilon_{p2}} \sigma d\varepsilon dx = \left(\frac{A\varepsilon_{p2}}{2} + \frac{B\varepsilon_{p2}^{\,n+1}}{(n+1)(n+2)} \right) (1 + C\log\dot{\varepsilon}_{p2})(D - E(T_{bulk}^{*})^m) \tag{29}$$

Assuming the mass passes the deformation zone under the DMZ is constant, the specific energy of the exit u_{p2exit} can be calculated as equal to $u_{p2entrance}$. The total specific energy of excess is represented as:

$$u_{p2} = u_{p2entrance} + u_{p2exit} \tag{30}$$

Specific Energy in Friction. A thin layer is normally considered between the DMZ and the workpiece. If the ratio of this layer thickness to the whole deformation area thickness is set as δ_2, δ_2 can taken as 0.10 (Zhang, et al., 1991). Also it is considered that along the DMZ boundary interface there is the sticking region and the shear stress is the shear flow stress k_{p3}. The strain-hardening effect is ignored as in treating the tool-chip interface, and the strain rate and the shear flow stress within the friction zone can be represented respectively as:

$$\dot{\varepsilon}_{p3} = \frac{V_{under}\cos(\alpha - \gamma)}{\sqrt{3}\delta_2 \lambda_{chamfer} \sin(\alpha - \beta)\sin\eta} \tag{31}$$

$$k_{p3} = A(1 + C\log\dot{\varepsilon}_{p3})(D - E(T_b^{*})^m)/\sqrt{3} \tag{32}$$

Using the hodograph in Fig 3, the velocity under the DMZ obeys the following relationship:

$$V_{under} = \frac{V\sin(\gamma + \eta)}{\sin\eta} \tag{33}$$

Since the power consumed per unit volume by the friction is calculated by the multiplication of the shear force and the velocity for a unit volume material, the specific energy for the friction is:

$$u_{p3} = \frac{k_{p3}\sin(\gamma + \eta)}{\sin^2\eta} \tag{34}$$

Computation Procedure

By given the cutting conditions and materials' properties, δ_1 is set as 0.05 (Ren, et al., 2000), and δ_2 as 0.1 (Zhang, et al., 1991). Shear angle ϕ will be found through iterations as in (Oxley, 1989). The reasonable values for C_{MN}, η, and γ are also searched iteratively at the same time, to simultaneously satisfy the condition $\sigma_{N1} = \sigma'_{N1}$, $\sigma_{N2} = \sigma'_{N2}$ as well as minimize $F_{c1} + F_{c2}$. When $F_{c1} + F_{c2}$ is minimized under a constant cutting speed, the minimum energy configuration has also been determined.

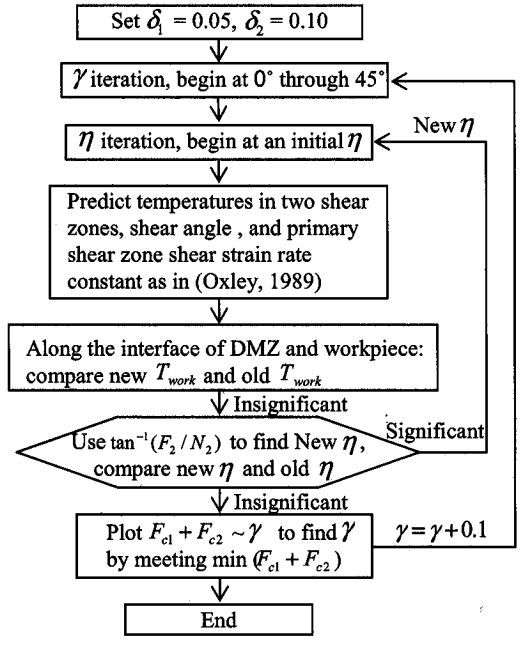

FIGURE 5. COMPUTATIONAL PROCEDURE FOR THE PROPOSED MODEL.

MODEL VALIDATION

Experimental results from (Ren, et al., 2000) are used to verify the proposed force modeling approach. The process conditions for this orthogonal machining were: workpiece material was P20 mold steel (HRc 34) with other physical

properties provided in (Ren, et al., 2000). Room temperature T_r is assumed as 20°C. Instead of using a power law as the workpiece flow stress model, a documented Johnson-Cook equation-based model (Shatla, et al., 2001) is used for P20 steel (HRc 30) in this study as follows: A = 145 Mpa, B = 565.6 Mpa, C = 0.03, D = 1.26, E = 1.07, n = 0.154, m=1.8, and Tm = 1480°C. The flow stress difference between these two P20 mold steels is considered negligible. Another P20 steel Johnson-Cook equation (Movahhedy, et al., 2002) has also been utilized to verify the model. Since the model predictions from these two material models are very similar, only the results from the former material model are presented in the following.

Effect of Cutting Speed

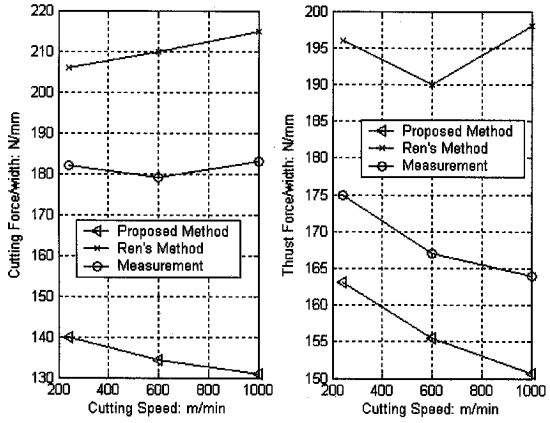

FIGURE 6. PREDICTED FORCES UNDER DIFFERENT CUTTING SPEEDS.

Cutting conditions in investigating the effect of cutting speed were (Ren, et al., 2000): the cut was orthogonal with feed of 0.06 mm/rev, depth of cut of 2.55 mm, and cutting speeds of 240, 600, 1000 m/min; the tool was MB820 CBN with rake angle -5°, chamfer angle -25°, and chamfer length 0.1 mm. It can be seen from Figure 6 that forces are all underestimated, but a satisfactory match is observed when the predicted thrust forces are compared with experimental measurements. Instead, Ren's model predictions (Ren, et al., 2000) are all overestimated. The proposed model predicts the thrust force better than that of Ren et al. (2000), although both modeling approaches are comparable in predicting the cutting force. Both predicted forces in this study decrease as cutting speed increases, and thrust force is sensitive to the cutting speed change. This decrease is assumed as the result of the thermal softening effect over the strain-hardening effect as cutting speed increases. However, different from the cutting force predictions, the measured cutting force decreases first, then increases after the speed is higher than 600 m/min. This contradictory observation needs further investigation in a future study. It is further found that cutting force is mainly contributed by the primary and secondary deformation zones and thrust force is mainly contributed by the deformation zone under the DMZ.

Effect of Chamfer Angle

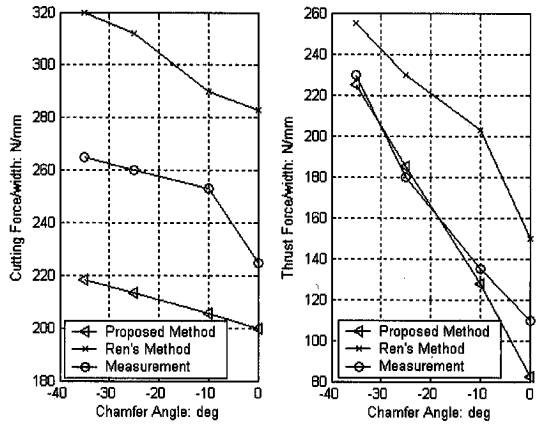

FIGURE 7. PREDICTED FORCES UNDER DIFFERENT CHAMFER ANGLES.

Cutting conditions in investigating the effect of chamfer angle were (Ren, et al., 2000): the cut was orthogonal with feed of 0.1 mm/rev, depth of cut of 3.6 mm, and cutting speed of 240 m/min; the tool was S10 carbide with tool geometry defined in (Ren, et al., 2000). It can be seen from Figure 7 that cutting force is underestimated, but thrust force is well predicted. Ren's model predictions (Ren, et al., 2000) are all overestimated on the effect of chamfer angle. Although both modeling approaches are comparable in predicting the cutting force and its tendency, the proposed model significantly improves the modeling capability in predicting the thrust force. All thrust forces decrease rapidly as the absolute value of chamfer angle decreases. It is suggested that this decrease is due to the decreased ploughing effect as the chamfer angle decreases. It is also further found that cutting force is mainly contributed by the primary and secondary deformation zones and thrust force is mainly contributed by the deformation zone under the DMZ. Figure 7 also shows that cutting force is not so sensitive to the chamfer angle change as

thrust force is.

DISCUSSION AND CONCLUSIONS

This paper presents a new force modeling approach in orthogonal cutting using chamfered tools. A three-zone model is improved to model the cutting process under the effect of the DMZ. The modeling performance is compared with that of Ren et al. (2000) in orthogonal cutting P20 mold steel, and overall an improved force modeling accuracy is observed. Although the predicted cutting force is lower than that of the measured, the predicted thrust force matches the measurement quite well. For the discussed validation cases, it is found that cutting force is mainly contributed by the primary and secondary deformation zones and thrust force is mainly contributed by the deformation zone under the DMZ. Since the proposed approach underestimates the cutting forces, a better understanding on the DMZ and the associated extrusion process needs further developments.

REFERENCES

Abebe, M., and F.C., Appl, (1981), "A Slip-line Solution for Negative Rake Angle Cutting," *Trans. of NAMRI/SME*, Vol. 19, pp. 341-348.

Chang, C.S., and K.H., Fuh, (1998), "An Experimental Study of the Chip Flow of Chamfered Main Cutting Edge Tools," *J. of Mat. Processing Tech.*, Vol. 73, pp. 167-178.

Hirao, M., J., Tlusty, R., Sowerby, and G., Chandra, (1982), "Chip Formation with Chamfered Tools," *J. of Eng. for Ind.*, Vol.104, pp. 339-342.

Hitomi, K., (1961), "Fundamental Machinability Research in Japan," *J. of Eng. for Ind.*, Vol. 83, pp.531-544

Huang, Y., (2002), *Predictive Modeling of Tool Wear Rate with Application to CBN Hard Turning*, Ph.D. Thesis, Georgia Institute of Technology, GA.

Huang, Y., and S.Y., Liang, (2003), "Cutting Forces Modeling Considering the Effect of Tool Thermal Property-Application to CBN Hard Turning," *Int. J. of Mach. Tools and Manuf.*, Vol. 43(3), pp. 307-315.

Jacobson, S., and P., Wallen, (1988), "A New Classification System for Dead Metal Zones in Metal Cutting," *Int. J. of Mach. Tools and Manuf.*, Vol. 28(4), pp.529-538.

Kita, Y., M., Ido, and N., Kawasaki, (1982), "A Study of Metal Flow Ahead of Tool Face with Large Negative Rake Angle," *J. of Eng. for Ind.*, Vol. (104), pp. 319-325.

Komanduri, R., and L.M., Raff, (2001), "A Review on the Molecular Dynamics Simulation of Machining at the Atomic Scale," *Proc. Instn. Mech. Engrs., Part B*, Vol. 215, pp. 1639- 1672.

Lortz, W., (1979), "A Model of the Cutting Mechanism in Grinding," *Wear*, Vol. 53, pp. 115-128.

Movahhedy, M.R., Y., Altintas, and M.S., Gadala, (2002), "Numerical Analysis of Metal Cutting with Chamfered and Blunt Tools," *ASME, J. of Manuf. Sci. & Eng.*, Vol. 124, pp. 178-188.

Oxley, P.L.B., (1989), *the Machanics of Machining: An Analytical Approach to Assessing Machinability*, Ellis Horwood Limited, England.

Ramesh, A., (2002), *Prediction of Process-Induced Mircrostructural Changes and Residual Stresses in Orthogonal Hard Machining*, Ph.D. Thesis, Georgia Institute of Technology, GA.

Ren, H., and Y., Altintas, (2000), "Mechanics of Machining with Chamfered Tools," *ASME, J. of Manuf. Sci. & Eng.*, Vol. 122, pp. 650-659.

Shatla, M., C., Kerk, and T., Alan, (2001), "Process Modeling in machining Part I: determination of flow stress data," *Int. J. of Mach. Tools and Manuf.*, Vol. 41, pp. 1511-1534.

Shaw, M.C. (1984), *Metal Cutting Principles*, Oxford University Press, England.

Waldorf, D.J., R.E., Devor, and S.G., Kapoor, (1998), "A Slip-line Field for Ploughing During Orthogonal Cutting," *ASME, J. of Manuf. Sci. & Eng.*, Vol. 120, pp. 693-699.

Waldorf, D.J., R.E., Devor, and S.G., Kapoor, (1999), "An Evaluation of Ploughing Models for Orthogonal Machining," *ASME, J. of Manuf. Sci. & Eng.*, Vol. 121, pp. 550-558.

Zhang, H.T., P.D., Liu, and R.S., Hu, (1991), "A three-zone model and solution of shear angle in orthogonal machining," *Wear*, Vol. 145, pp.29-43.